ACS APPLIED MATERIALS & INTERFACES

Research Article

www.acsami.org

Influence of Packing Density and Surface Roughness of Vertically-Aligned Carbon Nanotubes on Adhesive Properties of Gecko-Inspired Mimetics

Bingan Chen,[†,§] Guofang Zhong,*[,†] Pola Goldberg Oppenheimer,[‡] Can Zhang,[†] Hans Tornatzky,[†] Santiago Esconjauregui,[†] Stephan Hofmann,[†] and John Robertson[†]

[†]Department of Engineering, University of Cambridge, Cambridge, CB2 1PZ, United Kingdom

[‡]School of Chemical Engineering, University of Birmingham, Edgbaston, Birmingham, B15 2TT, United Kingdom

Supporting Information

ABSTRACT: We have systematically studied the macroscopic adhesive properties of vertically aligned nanotube arrays with various packing density and roughness. Using a tensile setup in shear and normal adhesion, we find that there exists a maximum packing density for nanotube arrays to have adhesive properties. Too highly packed tubes do not offer intertube space for tube bending and side-wall contact to surfaces, thus exhibiting no adhesive properties. Likewise, we also show that the surface roughness of the arrays strongly influences the adhesion properties and the reusability of the tubes. Increasing the surface roughness of the array strengthens the adhesion in the normal direction, but weakens it in the shear direction. Altogether, these results allow progress toward mimicking the gecko's vertical mobility.

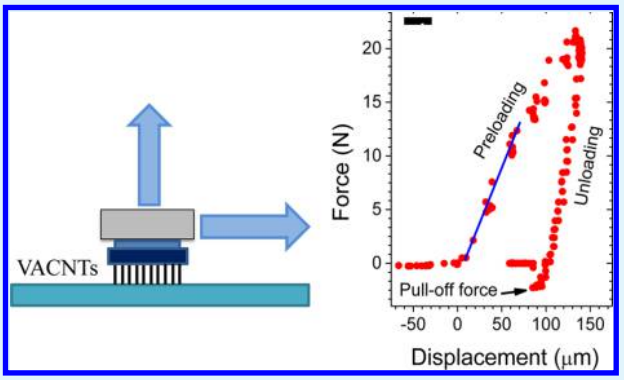

KEYWORDS: *carbon nanotube forests, dry adhesive, roughness, area density, packing density, shear adhesion, normal adhesion*

INTRODUCTION

Geckos have triggered extensive research owing to their extraordinary ability to stick to and climb up vertical surfaces, as well as to be suspended from ceilings by just a single toe. Such unique adhesive properties (~10 N/cm^2) are attributed to the microarrays comprising millions of elastic microhairs found on geckos' feet; the nanohairs split into nanometer spatulas and adhere to surfaces via weak van der Waals forces.[1,2] There have been numerous attempts to fabricate gecko-foot-like dry adhesives.[1,3−6] These bioinspired artificial analogues are of potential interest for applications in industrial fixtures,[7] tissue adhesives,[8] or climbing robots,[9] especially where traditional adhesives (e.g., glue or tape) have proved to be inadequate.[10] A suitable synthetic adhesive requires a design that ensures the structure intimately conforms to rough surfaces, while is rigid enough not to collapse under their own weight. In doing this, essential structural parameters including diameter, length, and aspect ratio of the hairs need to be optimized for the desired ultimate adhesive performance.[11] Other factors such as the hair area density also need to be considered. In arthropods with adhesive hairy pads (e.g., flies, beetles, and arachnids), the density of hairs increases with increasing the body weight.[12] The attachment strength is amplified by the number of single contact points, which provide a larger contact area to the target surface.

To date, the most developed artificial adhesives with highly dense nanometer hairs are based on arrays of polymer pillars and vertically aligned carbon nanotubes (VACNTs).[13−16] Unlike polymer-based structures, VACNTs create strong and reversible fibrillar adhesives with great durability, partly due to the superior structure and exceptional mechanical strength of CNTs.[5,6,16−21] CNT-based dry adhesives were first proposed by Yurdumakan et al., who measured the nanometer-scale adhesion force of VACNTs and found it is ~200 times higher than that of gecko foot hairs (>1.6 × 10^{-2} nN/nm^2).[17] Subsequently, Zhao et al. measured the macroscopic adhesion of VACNTs and found it is ~10 N/cm^2 against glass surface.[18] Further developments include micro patterned arrays of VACNTs by Ge et al.[19] In studying the adhesion/friction of the arrays against glass substrates, they found that the overall adhesion of compliant nanohairs increases with increasing the preload. This is because the increase deforms the arrays, thus continuously adding new side-wall nanotube contacts to the surface. The process appears to be very hysteretic with no real decrease in the actual area of contact until pull-off.[6] The performance of adhesion was then enhanced by Qu et al. using curly entangled end segments.[5] Although this proves a stronger shear adhesion, it weakens the normal adhesion. The mechanism of adhesion has been studied theoretically and in terms of tube properties such as wall number. Maeno et al.[22]

Received: November 10, 2014
Accepted: January 22, 2015
Published: January 22, 2015

DOI: 10.1021/am507822b
ACS Appl. Mater. Interfaces 2015, 7, 3626−3632

observed that the shear adhesion depends on the wall number and that a broad distribution of wall number produces the highest shear strength. Theoretical works have shown that laterally distributed segments play an essential role in achieving high force anisotropy between normal and shear directions.[5,23−26]

VACNTs for developing artificial adhesives are typically synthesized by chemical vapor deposition (CVD).[5,16−19,27] Most of the research on CNTs for adhesives has focused on understanding the adhesion mechanism, on how to maximize the adhesive performance, and on how to increase the reusability of the arrays. This has generated a large number of scientific publications in the field.[5,18−20,28] Most studies have focused on how the roughness of the target surfaces impacts on the adhesion strength.[29−34] Herein, we systematically investigate macroscopic adhesive properties of VACNTs focusing on area densities and surface roughness of the nanotube arrays. The area density of the VACNTs is controlled by varying the thickness of the metal catalyst and the CNT CVD conditions,[35−38] and measured by the weight gain method and liquid-induced compaction method.[37,39] The overall surface roughness is analyzed by atomic force microscopy (AFM). The adhesion tests are carried out by a tensile setup (Figure 1) which records the pull-off forces the VACNTs exert from the target surface, both in normal and shear directions. Our results show that both the area density and the surface roughness of VACNTs play an important role in the adhesion strength of VACNT-based adhesives and attachment repeatability. Altogether, these results clarify the influence of various individual and collective nanotube parameters and clarify somewhat contradictory results previously reported.

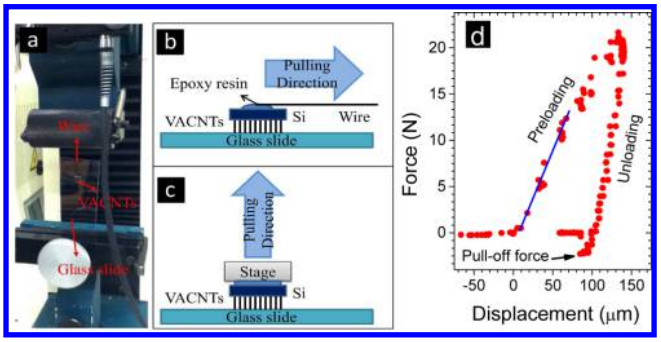

Figure 1. (a) Adhesion tests carried out using the tensile setup included a tensile machine under a shear test with the clamping of the sample wire at the upper stage and the clamping of the glass slide at the bottom. Schematic diagram of the VACNT surface subjected to the (b) shear and (c) normal tests on top of the glass slide. (d) Typical load versus displacement curve of normal adhesion test by tensile machine. The loading slope is used to calculate the effective Young's modulus, and the pull-off force is used as the adhesive force.

EXPERIMENTAL SECTION

We prepare four types of VACNTs with various area densities and nanotube lengths using 5 × 5 mm of Si substrates with thermally grown 200 nm of SiO_2 and a cold-wall CVD system. The nanotube area density (i.e., number of nanotubes per unit area) is evaluated by the weight gain method.[37] The packing density (i.e., the fraction of the area covered by tubes) is evaluated by liquid-induced compaction. It involves soaking the nanotube samples thoroughly in ethanol and letting them dry in air.[40−42] This causes the nanotubes to shrink into islands of closely packed tubes through the capillary force during the evaporation of the liquid between adjacent nanotubes.[37,43] The packing density is derived as the ratio of the top surface area of the tube islands to the original growth area (25 mm^2). The packing densities are 7, 15, 30, and 70% and the nanotube lengths range from 10 to 300 μm. Details of CVD conditions and area density measurements are given in the Supporting Information; Figure S1 shows top-view images of VACNTs after compaction.

Both shear and normal adhesion tests are performed using a tensile machine (Hounsfield 5kN), as shown in Figure 1a. We test a total of 60 nanotube array samples with different densities. For a shear test (Figure 1b), first a flexible wire is glued to the back side (Si) of a VACNT sample by epoxy resin. Then the sample is placed onto a glass slide and pressed by applying a constant force of 20 N normal to the glass slide to establish a good contact between the nanotubes and the target surface.[5,18] This process is called preloading. Finally, the wire is pulled at a constant rate of 0.5 mm/min under no external load until the VACNT sample detaches from the glass slide in a shear direction (parallel to the glass surface). For the normal test (Figure 1c), the back side of a VACNT sample is first attached to the upper stage by epoxy resin. After preloading the sample onto a glass slide by lowering the upper stage toward the glass slide until a force of 20 N is reached, the upper stage is then moved backward until the VACNT sample detaches from the glass slide. The detaching process is termed as the sample unloading. Figure 1d shows a typical force versus displacement curve obtained during the normal adhesion test with the preloading, unloading, and pull-off adhesion forces at which point the VACNT sample is detached from the glass slide and a maximum adhesive force is obtained. Both the shear and the normal adhesive forces are normalized by the area of the given substrate, yielding the shear (σ_c) and normal (σ_τ) adhesion strengths.

The surface morphologies of the VACNT adhesives before and after the adhesion tests are characterized by scanning electron microscope (SEM), and the surface roughness is measured by AFM. Here, we use the average surface roughness R_a, which is defined as the arithmetic average of absolute length difference of the CNTs from the mean length,[44] for roughness characterization:[45−48]

$$R_a = \frac{1}{n}\sum_{i=1}^{n} |\Delta h_i| \quad (1)$$

where, Δh_i is the vertical distance from the mean length to the i^{th} data point. The average surface roughness R_a is commonly used in researches of biomimetic adhesions although it is also seen the root-mean-square roughness (R_q).[31,49] R_q is defined as the value obtained from the deviations of the roughness profile over the net scan length, and has a linear relationship with R_a. From literature values and our case, (Figure S3, Supporting Information), we find $R_q \approx 1.1-1.3\ R_a$.[46,50] The advantage of AFM is that it can obtain the surface roughness at nanometer scale without damaging the samples. However, the disadvantage of our apparatus (dimension 3100 AFM) is that the scanning area is limited up to 50 × 50 μm. It is also time-consuming for such large areas. We find that R_a increases with the scanning area (Figure S4, Supporting Information). In this study, we optimize the scanning area to 25 × 25 μm for R_a measurements. It is kept constant for all evaluated samples, thus comparable among the experiments.

RESULTS AND DISCUSSION

The mechanism of adherence of VACNTs to surfaces is a complex process in which individual nanotube structural characteristics (diameter, length, or number of walls) as well as collective morphological properties of the arrays (area density and roughness of the contact surface) influence the adhesion performance. The roughness of the arrays can hardly be controlled during CNT CVD, so we have prepared a large number of samples to cover a wide range of roughness. In the first stage, we evaluate the influence of the area density of the arrays. We then check the results against array roughness, and

DOI: 10.1021/am507822b
ACS Appl. Mater. Interfaces 2015, 7, 3626−3632

interpret the results in a proposed adhesion mechanism. We present this in four subsections.

Influence of the Packing Density of the Arrays on Adhesion. We first test the adhesive properties of 60 different nanotube arrays with various area densities. We evaluate 16, 14, 20, and 10 VACNT samples with surface coverage of 7, 15, 30 and 70%, respectively. Half of the samples are for shear adhesion test, and half are for normal adhesion tests. The area densities range between 10^{10} and $\sim 10^{13}$ CNTs cm^{-2}. From these VACNTs, only the ultrahigh dense arrays ($> 5 \times 10^{12}$–10^{13} CNTs cm^{-2}) are formed by single-walled tubes.[37] The others arrays consist of multiwalled tubes with diameters between 7 and 15 nm. For this range of larger diameters, the area densities span from 10^{10} to $\sim 10^{11}$ CNTs cm^{-2}. The adhesion tests in both normal and shear directions reveal that highly compacted VACNTs present no adhesive properties. The result is consistently the same for the five analyzed samples. Conversely, all the less dense arrays show adhesion, with a tendency to increase the adhesion strength in both directions as the area density increases. For instance, the 7% coverage samples show a shear adhesive strength between ~2 and ~13 N/cm^2, and a normal adhesive strength between ~1 and ~5 N/cm^2, while the 30% samples show respectively between ~5 and ~19 N/cm^2 and between ~6 and ~12 N/cm^2.

To understand why highly packed nanotubes show no adhesion to surfaces, we observe the arrays before and after the preload process by high-resolution SEM (Figure 2). Side-view

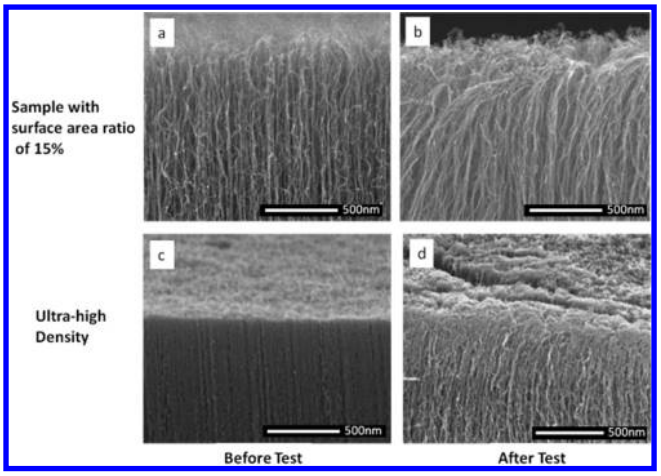

Figure 2. SEM images of the VACNTs (a and c) before and (b and d) after the adhesion tests. (a and b) Low-density VACNTs exhibit sufficient intertube space for the nanotubes to bend, resulting in a larger side-wall contact and increased adhesion, whereas (c and d) highly packed arrays have a very limited spacing for bending, resulting in a considerably reduced side-wall contact and consequently no adhesion at all.

SEM images show that ultradense arrays have practically no space in between the tubes for tube bending. This implies that only the nanotube tips, rather than the side-walls, can be in contact with a target surface. As the high adhesion of the CNTs to surfaces arises from side-wall contacts with target surfaces,[5] the arrangement of extremely packed tubes reduces or eliminates the adhesion properties of VACNTs. On this basis, we hypothesize that there exists an optimum range of VACNT density where the adhesion is maximized. The optimum value of area density appears to be between 10^{10} and $\sim 5 \times 10^{12}$ CNTs cm^{-2}. Higher area densities have a detrimental effect due to tube compaction. Lower densities might have good adhesives properties, but it is challenging to produce them. Very low-density nanotubes (<10^{10} CNT cm^{-2}) tend to grow randomly oriented and not vertically aligned to a support. We note that the effect of packing density applies regardless of the diameter and number of walls of the tubes. For any nanotube type, highly packed arrays will show no adhesion because there is no spacing between the tubes for them to bend and to adhere to surfaces. This is also in agreement with the peel-zone model described by Pesika et al.[51] that predicts the behavior of adhesives tapes at peel angles ≤90°. The model considers an angle-dependent multiplier to the Kendall equation that takes into account the geometrical changes within the peel zone. Highly packed arrays cannot produce the L-configuration necessary for the side contact to a target surface, therefore no peel angle (nor adherence) are verified.

Influence of Surface Roughness of the Arrays on Adhesion. In the second stage, we determine why VACNTs holding the same type of tubes and packing density show a wide range of adhesion values. We first analyze in detail the roughness of all VACNT arrays. Figure 3 shows how the

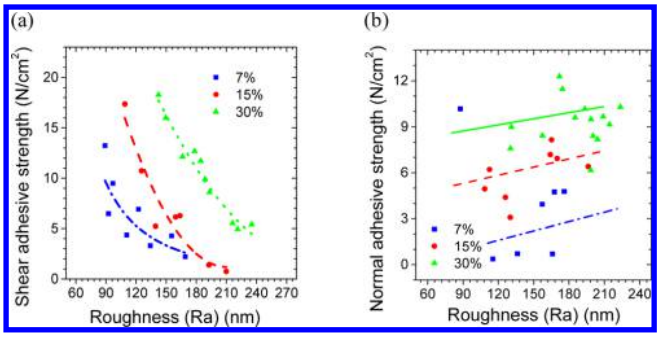

Figure 3. Dependence of (a) shear and (b) normal adhesion strength on the surface roughness of the VACNT samples; 7, 15, and 30% indicate the packing density of the arrays.

surface roughness of the VACNTs influences the adhesion strength. It can be seen that for a given VACNT packing density, the shear strength (σ_c) decreases dramatically with increasing the surface roughness (Figure 3a). The 30% packing density samples, for instance, show a shear adhesive strength of ~19 N/cm^2 when the roughness is ~140 nm, but it decreases to ~6 N/cm^2 when the roughness increases to ~230 nm. The behavior is different on the normal adhesion strength (σ_τ). It is found that σ_τ increases marginally with the surface roughness, showing nearly a slight increase within our experimental conditions (Figure 3b). The 30% packing density samples present a normal adhesive strength of ~7 N/cm^2 when the roughness is ~140 nm and it increases to ~10 N/cm^2 when the roughness is ~230 nm. In general, for a given roughness, both σ_c and σ_τ increase with increasing the area density of the VACNTs. On this basis, we argue the roughness of a nanotube array has a strong effect on both the shear and normal adhesion strength.

We then inspect by SEM the surface morphology of all samples (before and after the adhesion tests), Figure 4. The contact area of rough samples prior to tests exhibits a bumpy morphology (Figure 4a). After the normal adhesion test, the surface appears smoothened (Figure 4b). After the shear adhesion tests, we observe two types of tide-like morphologies, as shown in Figure 4c. The surface morphology shown in

DOI: 10.1021/am507822b
ACS Appl. Mater. Interfaces 2015, 7, 3626–3632

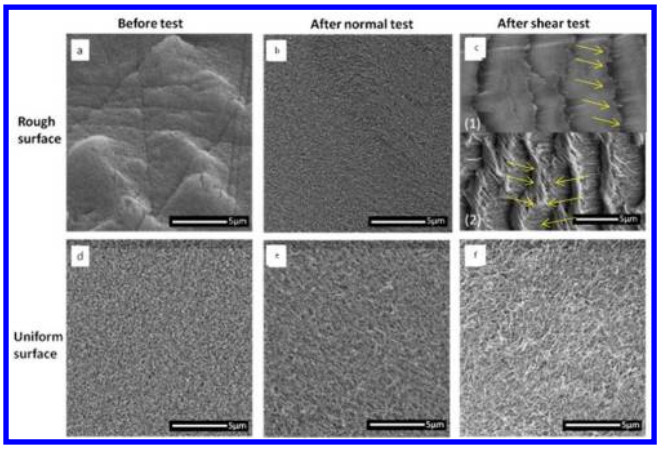

Figure 4. Top-view SEM images of VACNTs before and after adhesion tests. (a–c) are for rough surface samples and (d–f) for smooth surface samples.

Figure 4c1 is characterized by cracks (roughly perpendicular to the shearing direction) in which the tubes and their tips (indicated by arrows) are aligned in the shearing direction. This appears to occur when the arrays tilt toward the shearing direction during the preloading. The surface morphology shown in Figure 4c2 also consists of cracks (normal to the shear direction), but the tubes present a sickle shape instead (indicated by arrows). This appears to take place when the arrays tilt against the shearing direction during the preloading. The shearing motion results at the top part of the VACNTs bending along the shearing direction while the bottom part keeps tilted in the opposite direction. Note that array alignment toward or against the shearing direction takes place adventitiously when applying the force of 20 N during preloading. Due to a rough surface, the glass slide can slightly misalign, giving rise to array tilting. We have verified both possibilities of tube alignment by purposely preloading the glass slide with different angles. In contrast, VACNTs with a smooth surface retain their homogeneous surface morphology following both the shear and normal adhesion tests (Figure 4d–f). After shear tests, no cracks developed. All the tube tips are aligned in a single direction, regardless of whether the tubes themselves have aligned against or toward the shearing direction.

Roughness-Dependent Adhesion Model. Based on the two previous sets of data, we can now account for the effect of roughness on VACNT adherence to surfaces, as follows (Figure 5). Let us consider first the ideal case of a perfectly smooth array whose packing density allows tube bending (Figure 5a). All the tubes have the same length at the contact surface, and therefore, during preloading, they all contact the target surface with ideally the same side-wall contact area. During either shear or normal adhesion tests, the collective adhesion force has an equal contribution of each tube. All the tubes remain in contact with the surface until reaching the pull-off point. For a given packing density of VACNTs, the larger the contact area of each tube, the greater the adhesion force.

Conversely, when the VACNT arrays have a rough surface, the tubes exhibit local differences in height, at the contact area (Figure 5b). During preloading, the rough surface causes the tubes to tilt in a direction not always perpendicular to the glass slide. Following either test, the tubes detach upon reaching their limit of maximum stretching and elongation. We propose that because of the difference in height, the locally shorter tubes detach earlier than longer ones, thus originating a progressive tube detachment. This is reflected in a weaker adhesion force, thus explaining why the adhesion diminishes so dramatically as the roughness of the arrays increases. Such behavior can be visualized considering an extreme case of roughness, in which the local height difference exceeds the distance required for tube contact. Only a fraction of the tubes would adhere to a surface, and therefore, the total adhesion force would be weaker than that expected for the array with same packing density and smooth contact surface.

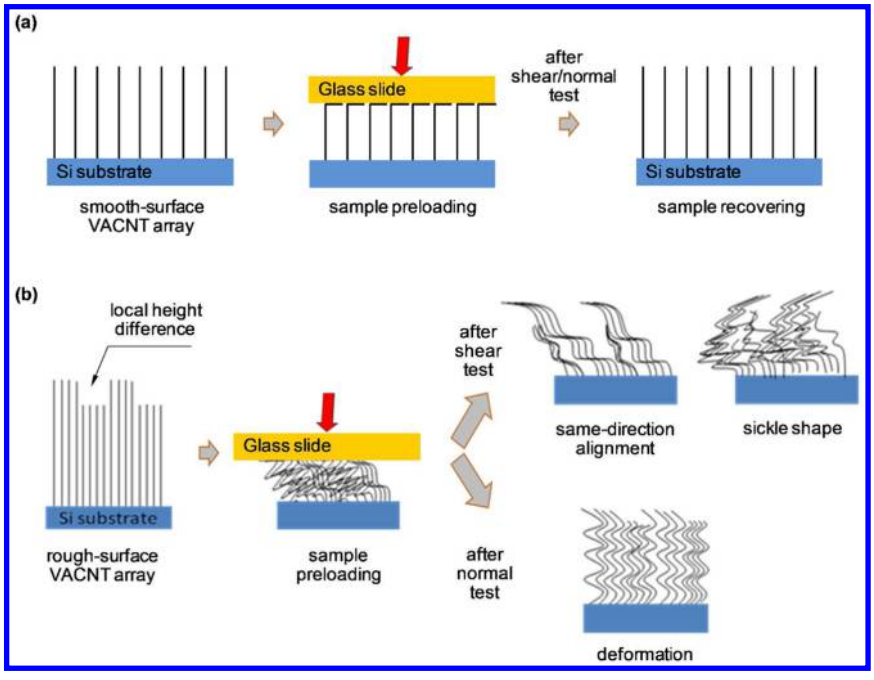

Figure 5. Cartoon of adhesion model depending on the surface roughness of an array of VACNTs: (a) smooth-surface and (b) rough-surface VACNT arrays.

DOI: 10.1021/am507822b
ACS Appl. Mater. Interfaces 2015, 7, 3626–3632

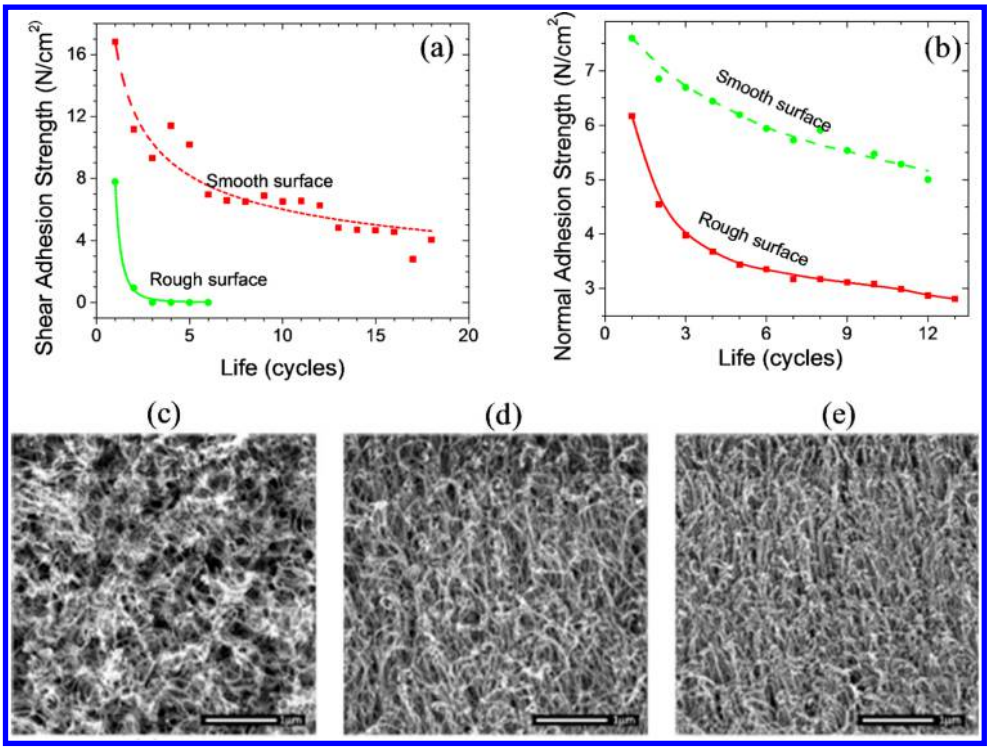

Figure 6. Shear strength measurements of (a) larger roughness VACNTs over 6 cycles compared with (b) low roughness substrate over 18 cycles and normal adhesion strength over 25 cycles for both low and large VACNTs surface roughess. Top-view SEM images of a low roughness VACNT substrate morphology (c) before the measurement, (d) after the 1st cycle, and (e) after the 15th cycle.

For the shear adhesion test, the detached shorter tubes get in the way of the still-on-contact longer ones. Eventually, upon reaching their elongation limit, the longer nanotubes also detach from the target surface, indicating the pull-off point. The partial tube detachment/bundling causes the cracks observed after shear tests. For the normal adhesion test, the mechanism is much simpler. Unloading of the samples perpendicular to the glass slide tends to restore the original growth direction of the VACNTs, despite any adventitious tube tilting during preloading. The restoration in the growth direction causes a plastic deformation of the tubes, resulting in a smoother surface after the pull-off point. This is probably why the surface roughness of the VACNTs has less effect on the normal adhesive strength than on shear adhesion. We note that despite the advances in VACNT synthesis by CVD, it is not yet possible to prespecify and produce nanotube arrays with a required roughness, in comparison to a required length or density.

Influence of the Packing Density of the Arrays on Cycle Life. The surface roughness is also found to be a factor that dramatically affects the adhesion life cycles and, thus, the reusability of the VACNT arrays. We investigate the structural integrity and adhesion durability of VACNTs (of the same packing density but different roughness) by repeating shear adhesion measurements over a number of cycles, as shown in Figure 6. Again, we observe two trends, depending on the surface roughness of the arrays. The plastic deformation of the CNTs with high surface roughness (R_a > 120 nm) causes the shear strength to decrease by a factor of 8 after the first test cycle, and then to remain constant (with a nearly no adhesion force) over the following five cycles (Figure 6a, scattered circles). The shear adhesion strength changes from ~8 N/cm^2 after the first cycle to ~1 N/cm^2 after the second cycle. This behavior arises from the tide-like morphology formed during the first cycle (Figure 4c). In changing the morphology, the tubes aggregate and form bundles, which results in a limited contact area with a target surface during the next preload process. In contrast, the shearing force in relatively smooth VACNTs ($R_a \leq$ 100 nm) decreases only by a factor of 3 after 10 cycles (Figure 6a, scattered squares). We observe a change in the shear adhesion strength from ~17 N/cm^2 after the first cycle to ~8 N/cm^2 after six cycles. This is because low-roughness-surface arrays retain the smooth top morphology following the typical attachment-detachment shearing cycle (Figure 4f). In the case of normal adhesion strength tests, the deformation/entanglement of the tubes is less pronounced than in shear tests. The repetition of cycles of stretching and compression in a normal direction leads to much less degradation of adhesion strength regardless of the type of array. As a result, the changes in normal adhesion strength are less abrupt. The smooth surface arrays, however, show a better performance. After 12 cycles, the normal adhesion strength changes from ~7 to ~5 N/cm^2 in smooth surface arrays, while for rough surface arrays, it changes from ~6 to ~2 N/cm^2.

These results highlight that it is yet necessary to improve the overall performance of adhesion in VACNTs. In order to closely mimic geckos' locomotion on vertical surfaces, an essential requirement for synthetic adhesives is to ensure an enduring adhesion, that is, their adherence performance must remain unchanged over a high number of cycles. VACNTs have to initially adhere to an upright surface (in the shearing direction) and then be pulled-off in the normal direction, while endeavoring to circumvent the formation of a tide-like morphology. Although the low roughness VACNTs exhibit a longer life-cycle, their pull-off strength reduces by more than a factor of 2 over several cycles. This is due to an increased self-

DOI: 10.1021/am507822b
ACS Appl. Mater. Interfaces 2015, 7, 3626−3632

entanglement of the tubes during each loading cycle.[52] Figure 6a,b suggest that most of the self-entanglement occurs during the first two cycles. These results are in agreement with previously reported structural changes on VACNTs following the preload process.[20] SEM images in Figure 6c–e show the morphological changes that VACNTs undergo after the adhesion tests. Sequential preloading steps cause nanotube entanglement followed by deformation after each reattachment. This consequently reduces the side-wall contact area of the VACNTs with the target surface. As a result, the adhesive strength diminishes after each cycle.

CONCLUSIONS

We have evaluated how the packing density and roughness of VACNT arrays influence the array adhesion to surfaces. We have found that there is a maximum packing density for arrays to be adhesive to a surface. Beyond that, no adhesion is possible, regardless of the nanotube properties. This is because highly packed tubes do not offer intertube space for tube bending and side-wall contact to target surfaces. We have also proven that the surface roughness of VACNTs is a highly important parameter for adherence and must be fully considered when designing gecko-mimetic adhesives. Adherence, especially in the shear direction, diminishes as the roughness of the arrays increases. This is because at their contact area the tubes possess locally different length, so that they adhere and detach from surfaces unevenly. In addition, the detachment creates cracks on the contact area and reduces considerably the reusability of VACNT-based adhesives. Altogether, these results clarify the influence of various individual and collective nanotube parameters and represent an improvement in understanding the mechanism of collective tube adhesion.

ASSOCIATED CONTENT

Supporting Information

Density variation and characterization of nanotube arrays by liquid-induced compaction method; roughness measurement by AFM; relationship between the root-mean-square roughness R_q and the average surface roughness R_a; surface roughness as a function of different scan size; and progressing reduction of the adhesive strength after consecutive cycles. This material is available free of charge via the Internet at http://pubs.acs.org.

AUTHOR INFORMATION

Corresponding Author

*E-mail: gz222@cam.ac.uk.

Present Address

[§]AIXTRON Ltd., Anderson Road, Buckingway Business Park, Swavesey, Cambridge CB24 4FQ, United Kingdom

Notes

The authors declare no competing financial interest.

ACKNOWLEDGMENTS

The authors acknowledge funding from the EC projects Technotubes and Grafol. We also thank J. J. Rickard of the Cavendish Laboratory for the use of AFM and Andrew Rayment in the Department of Materials Science and Metallurgy for the use of the tensile machine.

REFERENCES

(1) Autumn, K.; Liang, Y. A.; Hsieh, S. T.; Zesch, W.; Chan, W. P.; Kenny, T. W.; Fearing, R.; Full, R. J. Adhesive Force of a Single Gecko Foot-Hair. *Nature* **2000**, *405*, 681–685.

(2) Autumn, K.; Sitti, M.; Liang, Y. C. A.; Peattie, A. M.; Hansen, W. R.; Sponberg, S.; Kenny, T. W.; Fearing, R.; Israelachvili, J. N.; Full, R. J. Evidence for van der Waals Adhesion in Gecko Setae. *Proc. Natl. Acad. Sci. U.S.A.* **2002**, *99*, 12252–12256.

(3) Lee, H.; Lee, B. P.; Messersmith, P. B. A Reversible Wet/Dry Adhesive Inspired by Mussels and Geckos. *Nature* **2007**, *448*, 338–341.

(4) Greiner, C.; del Campo, A.; Arzt, E. Adhesion of Bioinspired Micropatterned Surfaces: Effects of Pillar Radius, Aspect Ratio, and Preload. *Langmuir* **2007**, *23*, 3495–3502.

(5) Qu, L. T.; Dai, L. M.; Stone, M.; Xia, Z. H.; Wang, Z. L. Carbon Nanotube Arrays with Strong Shear Binding-On and Easy Normal Lifting-Off. *Science* **2008**, *322*, 238–242.

(6) Ge, L. H.; Ci, L. J.; Goyal, A.; Shi, R.; Mahadevan, L.; Ajayan, P. M.; Dhinojwala, A. Cooperative Adhesion and Friction of Compliant Nanohairs. *Nano Lett.* **2010**, *10*, 4509–4513.

(7) Jeong, H. E.; Lee, J.-K.; Kim, H. N.; Moon, S. H.; Suh, K. Y. A Nontransferring Dry Adhesive with Hierarchical Polymer Nanohairs. *Proc. Natl. Acad. Sci. U.S.A.* **2009**, *106*, 5639–5644.

(8) Menciassi, A.; Dario, P. Bio-Inspired Solutions for Locomotion in the Gastrointestinal Tract: Background and Perspectives. *Philos. Trans. R. Soc. London, Ser. A* **2003**, *361*, 2287–2298.

(9) Kim, S.; Spenko, M.; Trujillo, S.; Heyneman, B.; Mattoli, V.; Cutkosky, M. R.; Whole Body Adhesion: Hierarchical, Directional, and Distributed Control of Adhesive Forces for a Climbing Robot, In Proceedings of the IEEE International Conference on Robotics and Automation, Rome, Italy, Apr 10–14; IEEE: New York, 2007; pp 1268–1273.

(10) Autumn, K.; Gravish, N. Gecko Adhesion: Evolutionary Nanotechnology. *Philos. Trans. R. Soc. London, Ser. A* **2008**, *366*, 1575–1590.

(11) Kamperman, M.; Kroner, E.; del Campo, A.; McMeeking, R. M.; Arzt, E. Functional Adhesive Surfaces with "Gecko" Effect: The Concept of Contact Splitting. *Adv. Eng. Mater.* **2010**, *12*, 335–348.

(12) Gorb, S. N.; Sinha, M.; Peressadko, A.; Daltorio, K. A.; Quinn, R. D. Insects Did It First: A Micropatterned Adhesive Tape for Robotic Applications. *Bioinspiration Biomimetics* **2007**, *2*, S117–S125.

(13) Sitti, M.; Fearing, R. S. Synthetic Gecko Foot-Hair Micro/Nano-Structures as Dry Adhesives. *J. Adhes. Sci. Technol.* **2003**, *17*, 1055–1073.

(14) Chan, E. P.; Greiner, C.; Arzt, E.; Crosby, A. J. Designing Model Systems for Enhanced Adhesion. *MRS Bull.* **2007**, *32*, 496–503.

(15) Autumn, K. Gecko Adhesion: Structure, Function, and Applications. *MRS Bull.* **2007**, *32*, 473–478.

(16) Chen, B. A.; Oppenheimer, P. G.; Shean, T. A. V.; Wirth, C. T.; Hofmann, S.; Robertson, J. Adhesive Properties of Gecko-Inspired Mimetic Via Micropatterned Carbon Nanotube Forests. *J. Phys. Chem. C* **2012**, *116*, 20047–20053.

(17) Yurdumakan, B.; Raravikar, N. R.; Ajayan, P. M.; Dhinojwala, A. Synthetic Gecko Foot-Hairs from Multiwalled Carbon Nanotubes. *Chem. Commun.* **2005**, 3799–3801.

(18) Zhao, Y.; Tong, T.; Delzeit, L.; Kashani, A.; Meyyappan, M.; Majumdar, A. Interfacial Energy and Strength of Multiwalled-Carbon-Nanotube-Based Dry Adhesive. *J. Vac. Sci. Technol., B* **2006**, *24*, 331–335.

(19) Ge, L.; Sethi, S.; Ci, L.; Ajayan, P. M.; Dhinojwala, A. Carbon Nanotube-Based Synthetic Gecko Tapes. *Proc. Natl. Acad. Sci. U.S.A.* **2007**, *104*, 10792–10795.

(20) Wirth, C. T.; Hofmann, S.; Robertson, J. Surface Properties of Vertically Aligned Carbon Nanotube Arrays. *Diamond Relat. Mater.* **2008**, *17*, 1518–1524.

(21) Tsai, Y. C.; Shih, W. P.; Wang, Y. M.; Huang, L. S.; Shih, P. J. E-Beam Photoresist and Carbon Nanotubes as Biomimetic Dry Adhesives. In *19th IEEE International Conference on Micro Electro*

DOI: 10.1021/am507822b
ACS Appl. Mater. Interfaces 2015, 7, 3626–3632

Mechanical Systems, Technical Digest, Istanbul, Turkey, Jan 22−26, 2006;IEEE: New York, 2006, pp 926929.
(22) Maeno, Y.; Nakayama, Y. Geckolike High Shear Strength by Carbon Nanotube Fiber Adhesives. *Appl. Phys. Lett.* **2009**, *94*.
(23) Hu, S. H.; Jiang, H. D.; Xia, Z. H.; Gao, X. S. Friction and Adhesion of Hierarchical Carbon Nanotube Structures for Biomimetic Dry Adhesives: Multiscale Modeling. *ACS Appl. Mater. Interfaces* **2010**, *2*, 2570−2578.
(24) Paudel, N. R.; Buldum, A.; Ohashi, T.; Dai, L. Modelling and Simulations of Adhesion between Carbon Nanotubes and Surfaces. *Mol. Simul.* **2009**, *35*, 520−524.
(25) Li, C. Y.; Chou, T. W. Modeling of Elastic Buckling of Carbon Nanotubes by Molecular Structural Mechanics Approach. *Mech. Mater.* **2004**, *36*, 1047−1055.
(26) Xia, Z.; Liang, J. Multiscale Modeling of Carbon Nanotube Adhesion for Dry Adhesives. *MRS Online Proc. Libr.* **2006**, *975*, DOI:10.1557/PROC-975-0975-DD10-09.
(27) Qu, L.; Dai, L. Gecko-Foot-Mimetic Aligned Single-Walled Carbon Nanotube Dry Adhesives with Unique Electrical and Thermal Properties. *Adv. Mater.* **2007**, *19*, 3844−+.
(28) Jeong, H. E.; Suh, K. Y. Nanohairs and Nanotubes: Efficient Structural Elements for Gecko-Inspired Artificial Dry Adhesives. *Nano Today* **2009**, *4*, 335−346.
(29) Canas, N.; Kamperman, M.; Voelker, B.; Kroner, E.; McMeeking, R. M.; Arzt, E. Effect of Nano- and Micro-Roughness on Adhesion of Bioinspired Micropatterned Surfaces. *Acta Biomater.* **2012**, *8*, 282−288.
(30) Persson, B. N. J.; Gorb, S. The Effect of Surface Roughness on the Adhesion of Elastic Plates with Application to Biological Systems. *J. Chem. Phys.* **2003**, *119*, 11437−11444.
(31) Huber, G.; Gorb, S. N.; Hosoda, N.; Spolenak, R.; Arzt, E. Influence of Surface Roughness on Gecko Adhesion. *Acta Biomater.* **2007**, *3*, 607−610.
(32) Kesari, H.; Doll, J. C.; Pruitt, B. L.; Cai, W.; Lew, A. J. Role of Surface Roughness in Hysteresis During Adhesive Elastic Contact. *Philos. Mag. Lett.* **2010**, *90*, 891−902.
(33) Quon, R. A.; Knarr, R. F.; Vanderlick, T. K. Measurement of the Deformation and Adhesion of Rough Solids in Contact. *J. Phys. Chem. B* **1999**, *103*, 5320−5327.
(34) Yu, J.; Chary, S.; Das, S.; Tamelier, J.; Turner, K. L.; Israelachvili, J. N. Friction and Adhesion of Gecko-Inspired PDMS Flaps on Rough Surfaces. *Langmuir* **2012**, *28*, 11527−11534.
(35) Komukai, T.; Aoki, K.; Furuta, H.; Furuta, M.; Oura, K.; Hirao, T. Density Control of Carbon Nanotubes through the Thickness of Fe/Al Multilayer Catalyst. *Jpn. J. Appl. Phys., Part 1* **2006**, *45*, 6043−6045.
(36) Xu, M.; Futaba, D. N.; Yumura, M.; Hata, K. Alignment Control of Carbon Nanotube Forest from Random to Nearly Perfectly Aligned by Utilizing the Crowding Effect. *ACS Nano* **2012**, *6*, 5837−5844.
(37) Zhong, G. F.; Warner, J. H.; Fouquet, M.; Robertson, A. W.; Chen, B. A.; Robertson, J. Growth of Ultrahigh Density Single-Walled Carbon Nanotube Forests by Improved Catalyst Design. *ACS Nano* **2012**, *6*, 2893−2903.
(38) Sakurai, S.; Inaguma, M.; Futaba, D. N.; Yumura, M.; Hata, K. Diameter and Density Control of Single-Walled Carbon Nanotube Forests by Modulating Ostwald Ripening through Decoupling the Catalyst Formation and Growth Processes. *Small* **2013**, *9*, 3584−3592.
(39) Robertson, J.; Zhong, G. F.; Esconjauregui, C. S.; Bayer, B. C.; Zhang, C.; Fouquet, M.; Hofmann, S. Applications of Carbon Nanotubes Grown by Chemical Vapor Deposition. *Jpn. J. Appl. Phys.* **2012**, *51*, 01AH01.
(40) Liu, H.; Li, S. H.; Zhai, J.; Li, H. J.; Zheng, Q. S.; Jiang, L.; Zhu, D. B. Self-Assembly of Large-Scale Micropatterns on Aligned Carbon Nanotube Films. *Angew. Chem., Int. Ed.* **2004**, *43*, 1146−1149.
(41) Chakrapani, N.; Wei, B. Q.; Carrillo, A.; Ajayan, P. M.; Kane, R. S. Capillarity-Driven Assembly of Two-Dimensional Cellular Carbon Nanotube Foams. *Proc. Natl. Acad. Sci. U.S.A.* **2004**, *101*, 4009−4012.
(42) Correa-Duarte, M. A.; Wagner, N.; Rojas-Chapana, J.; Morsczeck, C.; Thie, M.; Giersig, M. Fabrication and Biocompatibility of Carbon Nanotube-Based 3D Networks as Scaffolds for Cell Seeding and Growth. *Nano Lett.* **2004**, *4*, 2233−2236.
(43) Futaba, D. N.; Hata, K.; Yamada, T.; Hiraoka, T.; Hayamizu, Y.; Kakudate, Y.; Tanaike, O.; Hatori, H.; Yumura, M.; Iijima, S. Shape-Engineerable and Highly Densely Packed Single-Walled Carbon Nanotubes and Their Application as Super-Capacitor Electrodes. *Nat. Mater.* **2006**, *5*, 987−994.
(44) Gadelmawla, E. S.; Koura, M. M.; Maksoud, T. M. A.; Elewa, I. M.; Soliman, H. H. Roughness Parameters. *J. Mater. Process. Technol.* **2002**, *123*, 133−145.
(45) Gorb, S.; Varenberg, M.; Peressadko, A.; Tuma, J. Biomimetic Mushroom-Shaped Fibrillar Adhesive Microstructure. *J. R. Soc., Interface* **2007**, *4*, 271−275.
(46) Bullock, J. M. R.; Federle, W. The Effect of Surface Roughness on Claw and Adhesive Hair Performance in the Dock Beetle *Gastrophysa viridula*. *Insect Sci.* **2011**, *18*, 298−304.
(47) Tellez, J. P. D.; Krahn, J.; Menon, C. Characterization of Electro-Adhesives for Robotic Applications, In Proceedings of the 2011 IEEE International Conference on Robotics and Biomimetics (ROBIO), Dec 7−11, 2011; IEEE: New York, **2011**; pp 1867−1872.
(48) Lou, M. S.; Chen, J. C.; M, L. C. Surface Roughness Prediction Technique for CNC End-Milling. *J. Ind. Technol.* **1998**, *15*, 1−6.
(49) Zappone, B.; Rosenberg, K. J.; Israelachvili, J. Role of Nanometer Roughness on the Adhesion and Friction of a Rough Polymer Surface and a Molecularly Smooth Mica Surface. *Tribol. Lett.* **2007**, *26*, 191−201.
(50) Farshad, F.; Rieke, H.; Garber, J. New Developments in Surface Roughness Measurements, Characterization, and Modeling Fluid Flow in Pipe. *J. Pet. Sci. Eng.* **2001**, *29*, 139−150.
(51) Pesika, N. S.; Tian, Y.; Zhao, B. X.; Rosenberg, K.; Zeng, H. B.; McGuiggan, P.; Autumn, K.; Israelachvili, J. N. Peel-Zone Model of Tape Peeling Based on the Gecko Adhesive System. *J. Adhes.* **2007**, *83*, 383−401.
(52) Majidi, C.; Groff, R.; Fearing, R. S. Clumping and Packing of Nanohairs Manufactured by Nanocasting. *ASME Int. Mech. Eng. Congr. Expo.* **2004**, IMECE2004−62142.

DOI: 10.1021/am507822b
ACS Appl. Mater. Interfaces 2015, 7, 3626−3632